

Article

Ru-N-C Hybrid Nanocomposite for Ammonia Dehydrogenation: Influence of N-doping on Catalytic Activity

Nguyen Thi Bich Hien ^{1,2,†}, Hyo Young Kim ^{1,†}, Mina Jeon ¹, Jin Hee Lee ¹, Muhammad Ridwan ^{1,2}, Rizcky Tamarany ¹ and Chang Won Yoon ^{1,2,*}

¹ Fuel Cell Research Center, Korea Institute of Science and Technology, Seoul 136791, Korea; E-Mails: 513503@kist.re.kr (N.T.B.H.); 090755@kist.re.kr (H.Y.K.); 090809@kist.re.kr (M.J.); jinhee.lee@psi.ch (J.H.L.); 611012@kist.re.kr (M.R.); f06782@kist.re.kr (R.T.)

² Clean Energy and Chemical Engineering, Korea University of Science and Technology, Daejeon 34113, Korea

[†] These authors contributed equally to this work.

* Author to whom correspondence should be addressed; E-Mail: cwyoona@kist.re.kr; Tel.: +82-2-958-5262; Fax: +82-2-958-5199.

Academic Editor: Umit Demirci

Received: 19 April 2015 / Accepted: 3 June 2015 / Published: 10 June 2015

Abstract: For application to ammonia dehydrogenation, novel Ru-based heterogeneous catalysts, Ru-N-C and Ru-C, were synthesized via simple pyrolysis of a mixture of $\text{RuCl}_3 \cdot 6\text{H}_2\text{O}$ and carbon black with or without dicyandiamide as a nitrogen-containing precursor at 550 °C. Characterization of the prepared Ru-N-C and Ru-C catalysts via scanning transmission electron microscopy, in conjunction with energy dispersive X-ray spectroscopy, indicated the formation of hollow nanocomposites in which the average sizes of the Ru nanoparticles were 1.3 nm and 5.1 nm, respectively. Compared to Ru-C, the Ru-N-C nanocomposites not only proved to be highly active for ammonia dehydrogenation, giving rise to a NH_3 conversion of >99% at 550 °C, but also exhibited high durability. X-ray photoelectron spectroscopy revealed that the Ru active sites in Ru-N-C were electronically perturbed by the incorporated nitrogen atoms, which increased the Ru electron density and ultimately enhanced the catalyst activity.

Keywords: Ru-N-C; ammonia; dehydrogenation; N-doping; hollow graphitic structure; fuel cell

1. Introduction

To address the growing demand for clean and sustainable technologies for portable, automobile, and stationary fuel cell applications, the development of potentially feasible hydrogen storage materials has become a burgeoning field of research over the last decade. Relevant materials include metal hydrides [1,2], metal-organic frameworks [3–5], and chemical hydrides [6,7]. Among these materials, chemical hydrogen storage materials, such as sodium borohydride [8–10] and ammonia borane [11,12], are of particular interest because they can store a large quantity of hydrogen in a safe manner [8–12]. In addition to the solid materials, liquid or gaseous fuels, such as formic acid [13] and ammonia [14], are promising candidates for chemical hydrogen storage applicable to fuel cells since they can provide economically viable hydrogen storage and delivery methods for on-site power generation using existing infrastructure [15,16].

Ammonia, a gas that can be condensed under mild conditions (20 °C and 0.8 MPa), has attracted increasing attention as a hydrogen carrier due to its significantly high hydrogen storage density of 17.8 wt%; furthermore, hydrogen can be produced on demand from ammonia in the presence of an appropriate catalyst [14,17]. In addition, H₂-release from ammonia is essentially CO-free, which allows direct feeding of the product stream into polymer electrolyte membrane fuel cells (PEMFCs), which is a potential advantage over conventional hydrocarbon reforming that requires an expensive, external hydrogen purification system. Moreover, nitrogen gas, the spent-fuel produced upon ammonia dehydrogenation, can readily be regenerated into ammonia by the Haber-Bosch process [18].

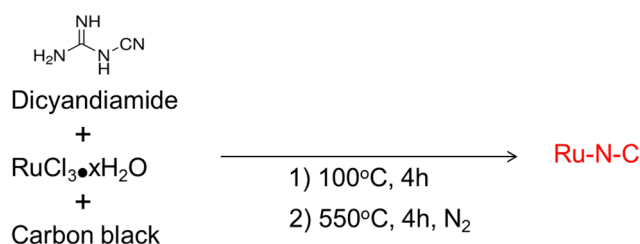
For ammonia to be useful in fuel cell applications, complete conversion (>99%) is required to circumvent poisoning of the PEMFC catalysts by unreacted ammonia, although an efficient adsorbent can decrease the quantity of residual ammonia to <200 ppb [19,20]. To achieve such high conversion, high reaction temperatures (>400 °C) are generally required to overcome the high activation barriers. In this context, numerous Ru-based heterogeneous catalysts, including Ru/carbon nanotubes (CNT) [21–25], Ru/Al₂O₃ [21,26–29], and Ru/SiO₂ [27] have been developed to promote ammonia dehydrogenation. Notably, Ru catalysts on carbon-based supports, such as CNTs and carbon nanofibers (CNFs), are highly active for the desired reaction. The activity of Ru/CNT [22,30] and Ru/CNF [31] has been further enhanced by increasing the charge density of the carbon supports via nitrogen doping. In addition to the catalysts for NH₃ decomposition, we recently developed a novel Fe-N-C electrocatalyst for the oxygen reduction reaction (ORR) that possesses a number of Fe-N-C interfaces [32]. In such nanostructures, the incorporated nitrogen atoms were proposed to donate electron density to the Fe metal centers, ultimately enhancing the ORR activity. The previous results obtained with the use of the N-doping strategy, along with our recent discovery, inspired us to develop a Ru-based catalyst supported on N-doped carbon materials given that the Ru-N-C interface is expected to provide improved catalyst activity and durability via the electronic interactions between Ru and the N-C sites.

In this contribution, we report the synthesis, characterization, and H₂-release properties of a Ru-N-C heterogeneous catalyst for ammonia dehydrogenation. The catalyst was prepared by pyrolysis of the precursors containing Ru, N, and C atoms. Numerous analytical techniques indicated the formation of hollow, hybrid nanostructures of Ru-N-C. In addition, the prepared Ru-N-C nanocomposite exhibited enhanced activity and durability compared to Ru-C at the temperatures ranging from 475 to 550 °C.

The influence of nitrogen doping on enhancing the catalytic performance of Ru-N-C was further proposed, based on the results obtained by a number of analyses.

2. Results and Discussion

Preparation of the Ru-N-C hybrid nanostructure was achieved by a modified procedure based on a previous report [32]. Ru metal ions were chemically chelated on carbon black spheres by thermal treatment of a mixture of dicyandiamide ($\text{HN}(\text{CN})_2$), RuCl_3 , and carbon in aqueous medium at 100 °C in air. The resulting Ru^{3+} -chelated composites were further calcined at 550 °C for 4 h in a N_2 atmosphere, which facilitated the formation of hybrid and graphitized Ru-N-C structures (Scheme 1). A possible mechanism for the formation of Ru-N-C is that the added $\text{Ru}^{3+}(\text{aq})$ ions could initially be interacted with nitrogen atom ($\text{HN}(\text{CN})_2$) at dicyandiamide via an attractive force between Ru^{3+} and nitrogen lone pairs. The weakly interacted species, $\text{Ru}^{3+}\text{-NH}(\text{CN})_2$ may then be transformed into the graphitized Ru-N-C structure in the presence of excess carbon species upon calcination at 550 °C by forming new chemical bonds between Ru-N and C via doping. Ru-C and C-N materials were likewise synthesized in the absence of the nitrogen-containing precursor, dicyandiamide, or RuCl_3 as control catalysts. The Ru content of the Ru-N-C and Ru-C materials were determined to be 0.97 wt% and 0.86 wt%, respectively, by using inductively coupled plasma optical emission spectroscopy (ICP-OES). In addition, the N content of Ru-N-C was found to be 14.2 wt%, as measured by SEM-EDX. The Ru, C and N contents of Ru-N-C and Ru-C are presented in Table S1.



Scheme 1. The synthetic procedure of Ru-N-C.

The transmission electron microscope (TEM) image of Ru-N-C demonstrates the formation of hollow graphitized structure even in the absence of a sacrificial template (Figure 1a,b); this approach to achieving such structures may potentially contribute to the reduction of chemical wastes [32] given that the formation of hollow carbon structures usually requires multistep processes with different templates [33,34]. The Ru-C catalyst also had a hollow structure, but aggregated Ru particles were observed with sizes of ~20 nm (Figure 1c,d). These results imply that the added nitrogen-containing precursor, dicyandiamide, facilitated uniform dispersion of the Ru species during pyrolysis. Given that Fe species promote the formation of hollow carbon nanostructures [32], the Ru species employed in the current synthetic procedure likewise played important roles in catalyzing the generation of hollow, N-doped graphitized nanostructures upon pyrolysis of the precursors containing carbon and/or nitrogen [35,36].

Elemental mapping of Ru-N-C using high-angle annular dark-field scanning transmission electron microscopy (HAADF-STEM) and energy-dispersive X-ray (EDX) indicated that Ru, C, and N were well dispersed over the catalyst (Figure 2, Figures S1 and S2). X-ray diffraction (XRD) analysis of Ru-N-C and Ru-C showed broadened peaks centered at 25.2° (Figure 3), which is attributed to the

graphitic stacking of C_3N_4 [37]. Ruthenium carbide, previously synthesized under high pressure (50,000 bar) and temperature (2000 K), appeared at 18.67° , 20.22° , and 21.23° [38]. Such peaks were not found in the XRD spectra, indicating that no ruthenium carbide species were formed under the reaction conditions employed in this study. A broad peak centered at 42.2° corresponding to metallic Ru was detected in the EDX profile of the Ru-N-C hybrid nanocomposite, indicating the formation of Ru nanoparticles with a size of 1.3 nm, calculated using the Scherrer equation. In contrast, additional sharp peaks centered at 38.5° , 44.2° , 58.5° , 69.7° , 78.7° , and 86.3° were observed in the spectrum of Ru-C, which are clearly attributed to the metallic Ru species (PDXL ver. 2.3.1). The average size of the Ru particles in Ru-C was likewise calculated to be 5.1 nm using the Scherrer equation, which is larger than that of the Ru particles in Ru-N-C. These results are consistent with the TEM observations (Figure 1b vs. 1d).

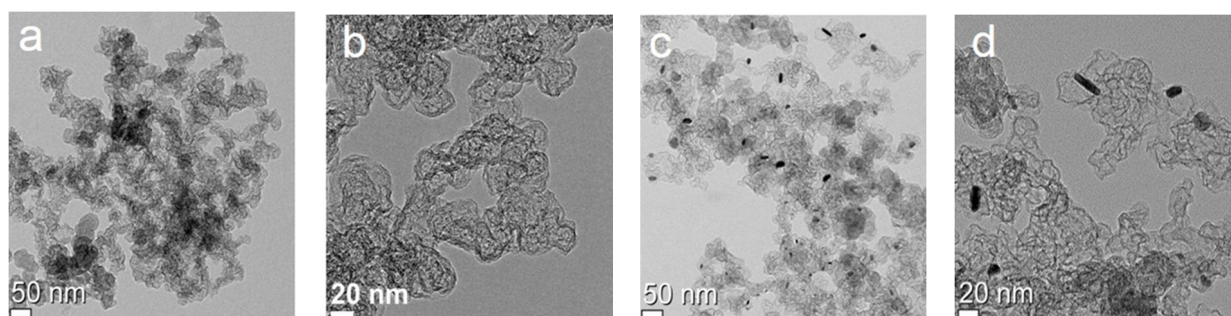


Figure 1. TEM images of the prepared catalysts: (a,b) Ru-N-C and (c,d) Ru-C.

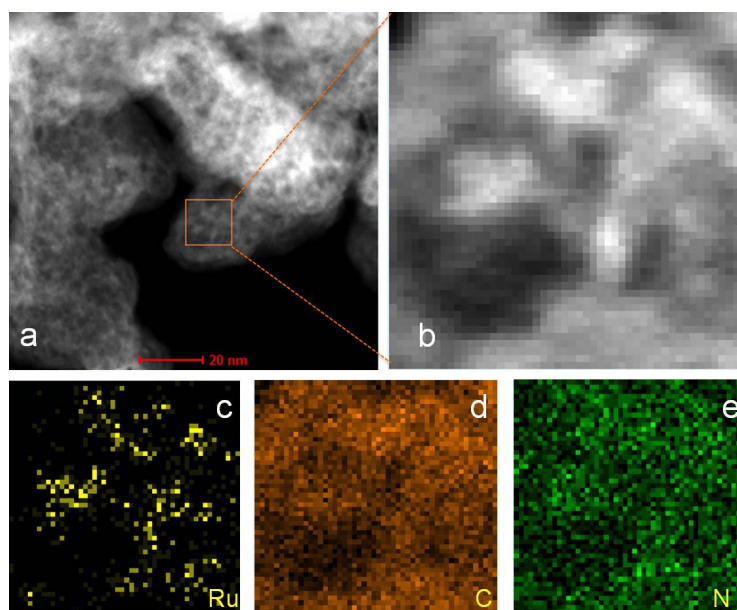


Figure 2. HAADF STEM images of: (a) Ru-N-C and (b) Ru-N-C with elemental mapping for (c) Ru; (d) C; and (e) N.

The textural properties of both catalysts were further determined from the N_2 adsorption–desorption isotherms. The BET surface area of Ru-N-C ($898 \text{ m}^2 \cdot \text{g}^{-1}$) was lower than that of Ru-C ($1110 \text{ m}^2 \cdot \text{g}^{-1}$) and there was also a slight reduction of the pore size and pore volume of Ru-N-C (Table 1). The stabilities of the as-prepared catalysts were also evaluated by thermogravimetric analysis (TGA). The TGA profile of Ru-N-C indicated reasonable stability up to 550°C , after which there was a sharp

loss of mass (Figure 4, red). The slight loss of mass at <100 °C is attributed to the desorption of adsorbed water species from the catalyst surface, while the sharp decrease beyond 550 °C may be associated with decomposition of the C-N support structure [39–41]. In contrast, decomposition of Ru-C was initiated at 380 °C, followed by a continual mass loss with increasing temperature (Figure 4, black) that may be attributable to collapse of the hollow carbon structure. The results suggest that the doped N atoms played an additional role in increasing the thermal stability of the catalyst, which can likely affect catalytic activity (*vide infra*).

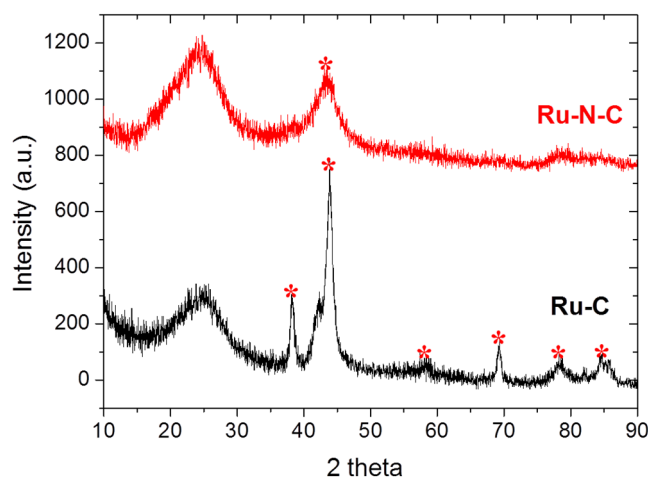


Figure 3. The XRD patterns of Ru-N-C (red) and Ru-C (black). The asterisk indicates Ru metallic phase.

Table 1. BET surface area, pore size, and pore volume of the Ru-based catalysts.

| Catalyst | BET Surface Area ^a (m ² ·g ^{−1}) | Pore Size ^a (nm) | Pore Volume ^a (cm ³ ·g ^{−1}) |
|----------|------------------------------------------------------------------|-----------------------------|--------------------------------------------------------------|
| Ru-N-C | 898 | 4.7 | 1.05 |
| Ru-C | 1110 | 5.4 | 1.57 |

Note: ^a Determined by physical N₂ adsorption-desorption isotherm.

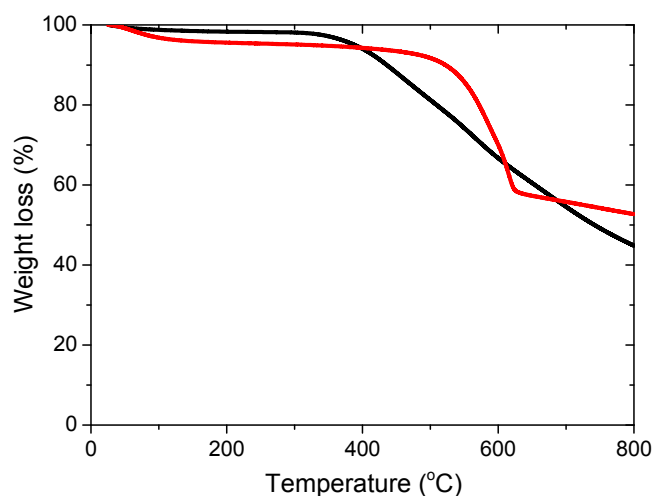


Figure 4. The TGA pattern of the Ru-N-C (red) and Ru-C (black) catalysts.

XPS was employed to determine the electronic state of the elements present in the Ru-C and Ru-N-C hybrid nanocomposites. The deconvoluted C 1s XPS spectrum of Ru-C displayed a narrow sp^2

graphitic peak centered at 284.6 eV (Figure 5a). Additional peaks for C-O species were found in the range of 284–290 eV, which presumably originated from adsorbed oxygen species from the precursor employed [42–44]. In the case of the Ru 3p state, a dominant peak centered at 463.3 eV was observed in the deconvoluted spectrum of Ru-C (Figure 5b), which is likely attributed to the RuO₂ phase [31]. An additional peak was observed at 466.1 eV for the Ru-C catalyst, presumably corresponding to RuO₂·xH₂O [31]. The Ru 3d spectrum of Ru-C exhibits a single peak centered at 281.2 eV (Figure S3a).

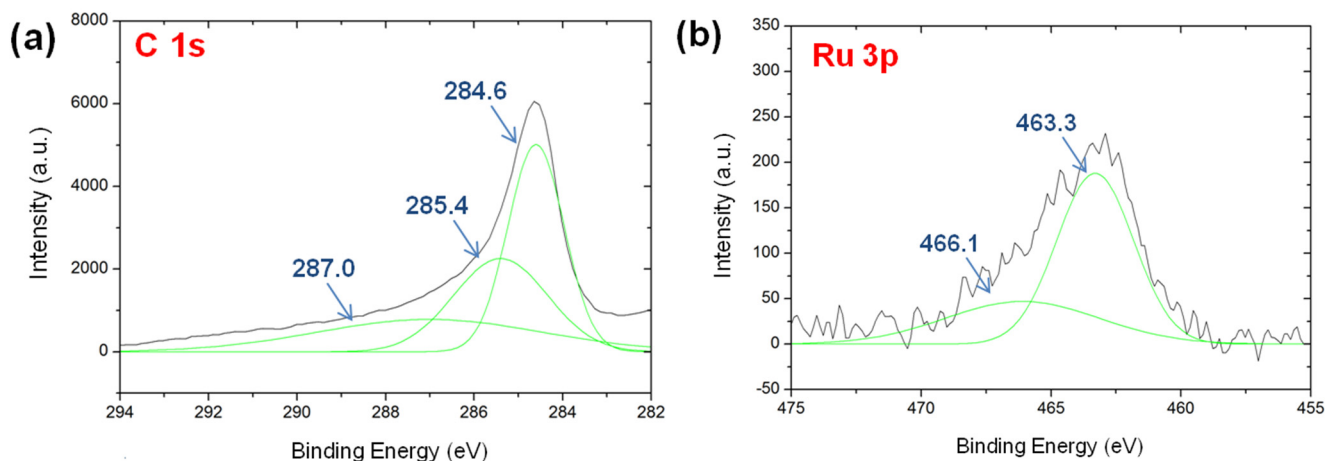


Figure 5. The XPS spectra of Ru-C: (a) C 1s and (b) Ru 3p.

Similar to the case of Ru-C, a dominant, narrow sp^2 graphitic carbon peak centered at 284.6 was found in the XPS spectrum of Ru-N-C (Figure 6a). Other peaks were also detected at 285–290 eV. In contrast to the peaks observed for Ru-C, these peaks may be derived from the formation of carbon species possessing $C(sp^2)$ -N and $C(sp^3)$ -N networks [45], indicating that nitrogen atoms were introduced into the graphitic structure upon pyrolysis. Moreover, Ru-N-C exhibited dominant N 1s peaks at binding energies ranging from 396 to 408 eV (Figure 6b), suggesting the formation of pyridinic-, nitrile-, pyrrolic-, and/or graphitic-like nitrogen species [32,45,46]. The Ru 3p XPS spectrum of Ru-N-C showed a major peak centered at 462.7 eV (Figure 6c). Notably, the peak at 462.7 eV for Ru-N-C appeared at lower binding energy compared to that of Ru-C, suggesting that the incorporated nitrogen atoms donated electron density into the Ru active sites. Ru-N-C also presented a broad peak centered at 466.6 eV, again attributable to RuO₂·xH₂O. As in the case of the Ru 3p spectrum, the Ru 3d peak of Ru-N-C occurred at a slightly lower binding energy (281.0 eV) than that of Ru-C (Figure S3b), again supporting the proposed electron transfer from N to Ru in the Ru-N-C nanocomposite.

The increased Ru electron density in Ru-N-C induced by nitrogen doping could potentially improve the activity and durability of the catalyst for NH₃ dehydrogenation, although its surface area is lower than that of Ru-C. To prove this hypothesis, the H₂-release properties of the as-developed catalysts were evaluated by varying the temperature and/or GHSV. Nearly exclusive ammonia dehydrogenation ($\geq 98\%$) is thermodynamically achievable even at temperatures as low as 425 °C [47]. In addition, the equilibrium ammonia conversion at 500 °C and 1 bar is close to 99.7% [15]. Due to the high kinetic barrier, however, only a limited number of catalysts show high activity at ≤ 500 °C. We initially assessed the catalytic activity of the as-prepared Ru catalysts for ammonia dehydrogenation as a function of temperature. As depicted in Figure 7, the activity of Ru-N-C proved to be higher than that of Ru-C at temperatures ranging from 475 to 550 °C. For example, at 550 °C, 95% NH₃ conversion

was achieved with Ru-N-C versus 68% conversion obtained with Ru-C. The conversion obtained at 500 °C with Ru-N-C (56%) was likewise found to be higher than that with Ru-C (20%). In the presence of C-N, negligible dehydrogenation activity was found at temperatures ≤ 600 °C (Figure 7, green triangles). For all the catalysts, the ammonia conversion increased with increasing temperature (Table S2), which is congruent with the endothermic nature of the dehydrogenation process.

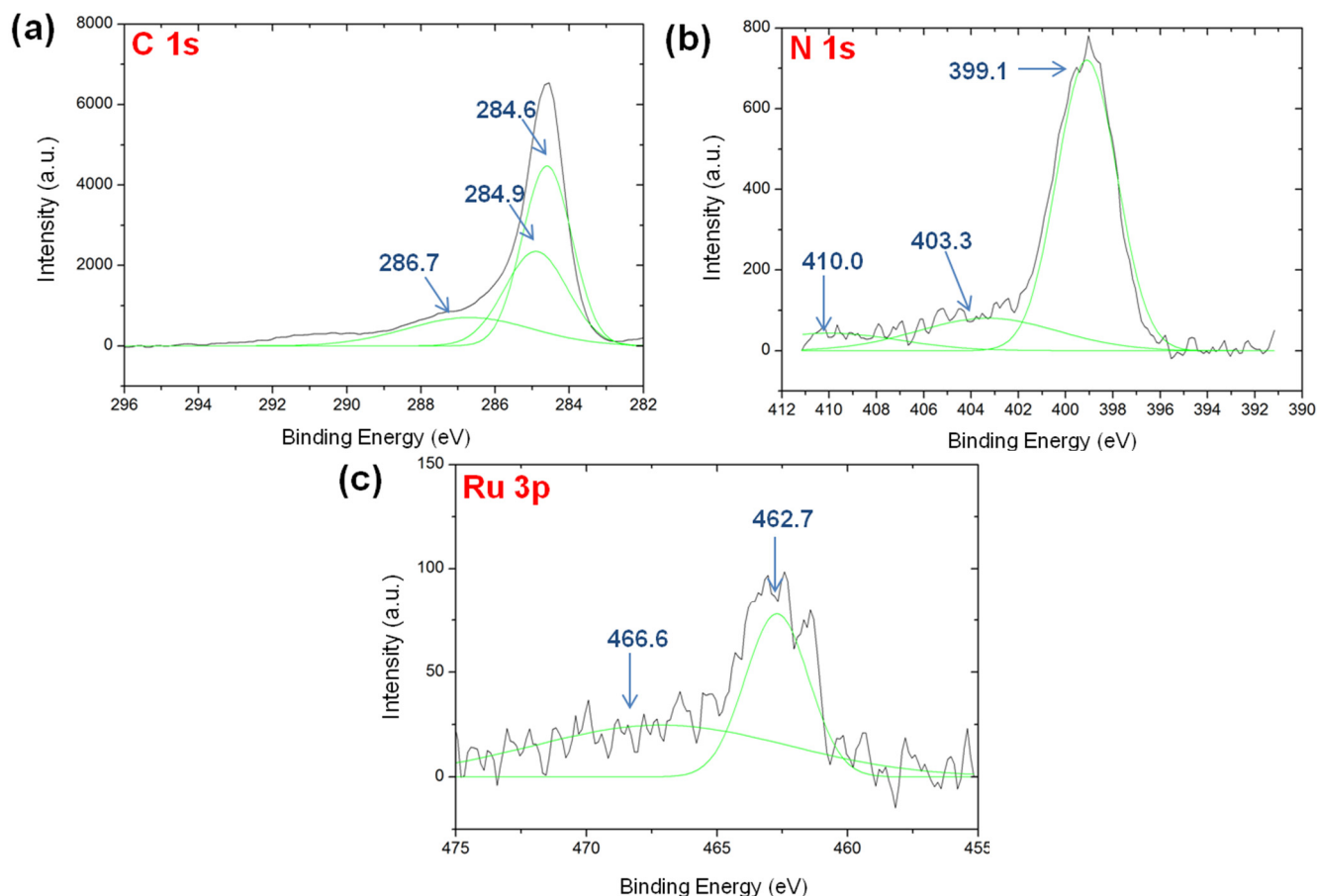


Figure 6. The XPS spectra of Ru-N-C: (a) C 1s; (b) N 1s; and (c) Ru 3p.

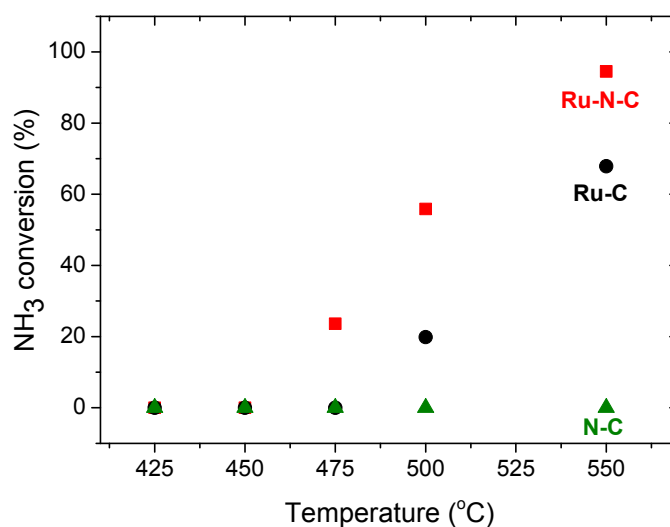


Figure 7. NH₃ conversion with Ru-N-C (■); Ru-C (●) and C-N (▲) at a GHSV of 7448 mL·g⁻¹·h⁻¹.

Since the Ru-N-C hybrid nanocomposite showed enhanced activity compared to Ru-C, the influence of the GHSV on NH_3 dehydrogenation in the presence of Ru-N-C was evaluated at different temperatures. As illustrated in Figure 8, the NH_3 conversion obtained with Ru-N-C declined as the GHSV increased at all temperatures employed (Table 2). Compared to the NH_3 conversion achieved with Ru-N-C at 550 °C using a GHSV of 2234 $\text{mL}\cdot\text{g}^{-1}\cdot\text{h}^{-1}$ (>99%), the NH_3 conversion decreased slightly to 94.5% when the GHSV was increased to 7448 $\text{mL}\cdot\text{g}^{-1}\cdot\text{h}^{-1}$. With a further increase of the GHSV to 11,172 $\text{mL}\cdot\text{g}^{-1}\cdot\text{h}^{-1}$ at 550 °C, the Ru-N-C catalyst still exhibited a high conversion of 81.5%. However, the decrease in NH_3 conversion observed for Ru-N-C with increasing GHSV was found to be pronounced at temperatures of 450 °C and 500 °C. The conversion (45%) achieved with a GHSV of 2234 $\text{mL}\cdot\text{g}^{-1}\cdot\text{h}^{-1}$ decreased to 0% at 450 °C upon utilization of a GHSV of 7448 $\text{mL}\cdot\text{g}^{-1}\cdot\text{h}^{-1}$. Likewise, the conversion (>97%) acquired using a GHSV of 2234 $\text{mL}\cdot\text{g}^{-1}\cdot\text{h}^{-1}$ decreased to 31% at 500 °C when a GHSV of 11,172 $\text{mL}\cdot\text{g}^{-1}\cdot\text{h}^{-1}$ was employed. Based on the results described above, it is reasonable that the improved activity for H_2 -release from NH_3 over Ru-N-C may originate from the incorporation of nitrogen species that contributed to: (i) the formation of the small-sized Ru nanoparticles by initially anchoring the Ru^{3+} precursor to prevent them from sintering (Figure 1); (ii) enhancing the thermal stability of the catalyst (Figure 4); and (iii) increasing the Ru electron density induced by the interaction between Ru and N (Figure 6).

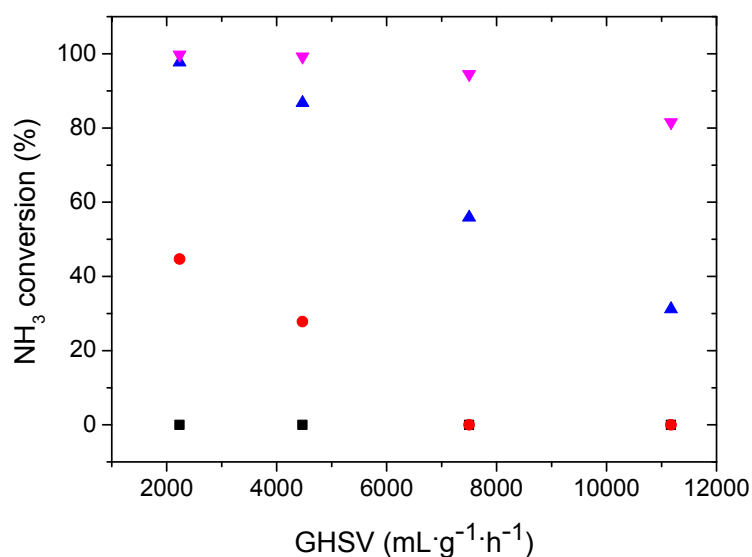


Figure 8. The influence of GHSV on NH_3 dehydrogenation over Ru-N-C at different temperatures: (■) 400 °C; (●) 450 °C; (▲) 500 °C; and (▼) 550 °C.

Table 2. The NH_3 conversions of Ru-N-C as functions of GHSV and temperature.

| GHSV | 400 °C | 450 °C | 500 °C | 550 °C |
|--------|--------|--------|--------|--------|
| 2234 | 0 | 44.7 | 97.7 | 99.7 |
| 4469 | 0 | 27.8 | 86.8 | 99.2 |
| 7448 | 0 | 0 | 55.9 | 94.5 |
| 11,172 | 0 | 0 | 31.2 | 81.5 |

Long-term stability is a desirable property for a number of catalytic applications. In this context, long-term experiments with Ru-N-C were carried out under dehydrogenation conditions employing a GHSV of $7448 \text{ mL}\cdot\text{g}^{-1}\cdot\text{h}^{-1}$ and temperatures of 500°C and 550°C . Initially at 550°C , the initial NH_3 conversion of 95% obtained with Ru-N-C decreased slightly to 88% after 80 h (Figure S4). Upon dehydrogenation at 500°C , the initial NH_3 conversion of ca. 60% was maintained for 80 h without apparent deactivation (Figure 9, red). Surprisingly however, the initial NH_3 conversion of 19% obtained with Ru-C increased gradually to 36% after 80 h under the identical conditions (Figure 9, black). Considering that NH_3 has previously been employed as the N-doping agent for carbon nanotubes [22,30], the unexpected, increased activity of Ru-C strongly suggests the transformation of Ru-C into a N-incorporated Ru-C structure analogous to that of Ru-N-C via N-doping upon NH_3 dehydrogenation.

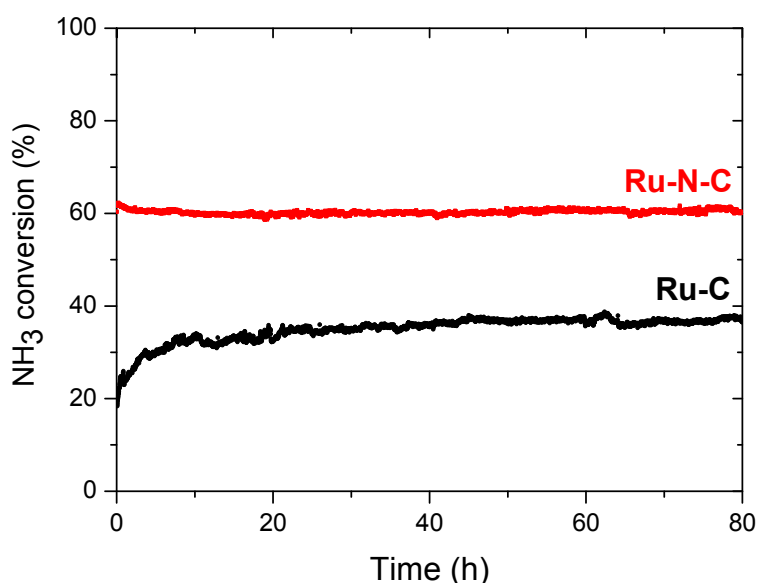


Figure 9. Long term stability for NH_3 dehydrogenation at 500°C , with a GHSV of $7448 \text{ mL}\cdot\text{g}^{-1}\cdot\text{h}^{-1}$, obtained by: Ru-N-C (■) and Ru-C (●).

Consistently, elemental mapping with the spent Ru-C catalyst, obtained at randomly selected four different areas, revealed the presence of N element over Ru-C with an average quantity of 0.82 wt% (Figure 10 and Figure S5), again confirming the incorporation of N atoms into Ru-C during NH_3 dehydrogenation. The results suggest that the as-developed Ru-N-C catalyst could be employed for a long-term fuel cell application.

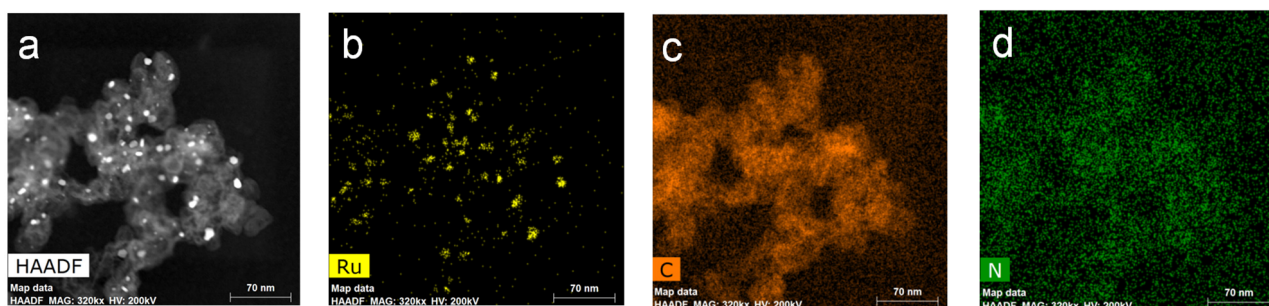


Figure 10. (a) HAADF STEM images of Ru-C following the long-term stability test for 80 h and elemental mapping with (b) Ru; (c) C; and (d) N.

3. Experimental Section

3.1. Synthesis of Ru-N-C, Ru-C, and C-N Materials

$\text{RuCl}_3 \cdot x\text{H}_2\text{O}$ (0.25 g, Sigma-Aldrich, St. Louis, MO, USA), carbon black (1.0 g, Ketjen, Akzo Nobel, Chicago, IL, USA), and dicyandiamide (1.0 g, Sigma-Aldrich, St. Louis, MO, USA) were combined with distilled water (50 mL), followed by heating at 100 °C for 4 h with vigorous stirring to vaporize water. The resulting black solids obtained subsequent to complete drying were ground and pyrolyzed at 550 °C for 4 h under a N_2 flow, yielding the final product, Ru-N-C as a black powder. The Ru-C and C-N materials were also synthesized using an otherwise identical procedure except for the absence of either dicyandiamide or $\text{RuCl}_3 \cdot x\text{H}_2\text{O}$. The schematic synthetic procedure is depicted in Scheme 1.

3.2. Catalytic NH_3 Dehydrogenation

The performance of the catalyst was evaluated under a flow of 10% NH_3/N_2 at a rate of $37.2 \text{ mL} \cdot \text{min}^{-1}$ at atmospheric pressure using a fixed-bed quartz reactor. In a typical experiment, the catalyst (0.1 g, 0.05 g, 0.03 g, 0.01 g; 100–150 μm) was positioned in the reactor, followed by reduction using 50% H_2/N_2 at a flow rate of $30 \text{ mL} \cdot \text{min}^{-1}$ using a temperature of 550 °C and a duration of 1 h. The in-situ reduced catalyst was then flushed with N_2 for 1 h, and the NH_3 dehydrogenation reactions were then executed at temperatures ranging from 550 to 450 °C while decreasing the temperature in 25 °C increments. The compositions of the effluent gases were determined by using an online gas chromatograph (Agilent 7890A, Santa Clara, CA, USA) equipped with Porapak Q and Molecular sieve capillary columns as well as a thermal conductivity detector (TCD, Agilent, Santa Clara, CA, USA). The content of unreacted NH_3 was analyzed using a tunable diode laser ammonia gas analyzer (Model Airwell+7, KINSCO Technology, Seoul, Korea). The dehydrogenation activity of the catalysts was monitored as a function of the GHSV and the temperature.

3.3. Catalyst Characterization

The crystalline patterns of the as-prepared materials were initially determined by XRD studies using a Rigaku X-ray diffractometer with $\text{CuK}\alpha$ radiation at 40 kV and 20 mA. Continuous scanning at a rate of $0.5^\circ \cdot \text{min}^{-1}$ was performed in the 2θ range of 20° – 80° . The specific surface area, pore size, and pore volume of the materials were determined using a nitrogen adsorption instrument (Micrometrics ASAP 2000, Dr. Norcross, GA, USA) at 77 K. The thermal stability of the catalysts was evaluated by TGA at a heating rate of $10^\circ \text{C} \cdot \text{min}^{-1}$ in the temperature range of 25–1000 °C.

The morphology of the synthesized catalysts was characterized using a HRTEM (FEI Tecnai F20, FEI Corporate, Hillsboro, OR, USA) and a HAADF-STEM (FEI Titan, FEI Corporate, Hillsboro, OR, USA) at 200 kV. Electron energy loss spectra (EELS) of C (K edge, 284 eV), N (K edge, 401 eV), and Fe (L3 edge 708 eV) were collected by using a Quantum 996 instrument (Quantum instrument, Bartlett, IL, USA) to determine the atomic distribution of the elements.

The electronic structure and local bonding environment of Ru-N-C were further identified by using an XPS instrument equipped with a PHI 50000 Versa Probe (Ulvac-PHI, Kanagawa, Japan) using a

monochromated Al K α X-ray (1486.6 eV) beam calibrated by the C 1s peak (284.6 eV) with a background pressure of 6.7×10^{-8} Pa. The Ru contents of the catalytic materials were determined by means of inductively coupled plasma-optical emission spectrometry (ICP-OES) (Varian 720ES Agilent, Santa Clara, CA, USA) and scanning electron microscopy-energy dispersive X-ray (SEM-EDX, FEI Corporate, Hillsboro, OR, USA) analysis. CO chemisorption experiments were conducted to evaluate the Ru dispersion.

4. Conclusions

The simple synthetic strategy presented herein provides an economical route for large-scale production of the highly active Ru-N-C catalyst. The Ru-N-C catalyst displayed excellent performance for NH₃ dehydrogenation with high stability. The incorporated nitrogen atoms were proposed to play pivotal roles in: (i) generating uniformly distributed, small-sized Ru nanoparticles; (ii) improving the thermal stability of the catalyst; and (iii) donating electron density to Ru via electronic interactions between Ru and N. For the undoped Ru-C catalyst, the reactant NH₃ further revealed to act as a N-doping agent to convert Ru-C into N-doped Ru-C structure during NH₃ dehydrogenation, which ultimately enhancing the desired activity. The as-developed Ru-N-C hybrid nanocomposite is thus applicable for on-site hydrogen production from ammonia with relevant catalyst optimization, and further provides insight for the development of various M-N-C catalysts (M = transition metals) for a number of chemical transformations.

Supplementary Materials

Supplementary materials can be accessed at: <http://www.mdpi.com/1996-1944/8/6/3442/s1>.

Acknowledgments

This work was supported by the New and Renewable Energy Core Technology Program of the Korea Institute of Energy Technology Evaluation and Planning (KETEP), granted financial resource from the Ministry of Trade, Industry and Energy, Republic of Korea (No. 20143030031360). Part of the research is also supported by the Global Research Laboratory Program through the National Research Foundation of Korea funded by the Ministry of Science, ICT and Future Planning of Republic of Korea as well as basic research program from Korea Institute of Science and Technology.

Author Contributions

Nguyen Thi Bich Hien and Hyo Young Kim contributed equally to this original research paper. They prepared and characterized the catalysts, and contributed to the major part of manuscript writing. Mina Jeon and Jin Hee Lee evaluated the activity of the catalysts during ammonia dehydrogenation over the catalysts. Muhammad Ridwan and Rizcky Tamarany contributed to interpretation of the obtained data and critique of the manuscript. Chang Won Yoon contributed to the conception and design of the research concept as well as to overseeing manuscript writing.

Conflicts of Interest

The authors declare no conflict of interest.

References

1. Adelhelm, P.; de Jongh, P.E. The impact of carbon materials on the hydrogen storage properties of light metal hydrides. *J. Mater. Chem.* **2011**, *21*, 2417–2427.
2. Orimo, S.-I.; Nakamori, Y.; Eliseo, J.R.; Züttel, A.; Jensen, C.M. Complex hydrides for hydrogen storage. *Chem. Rev.* **2007**, *107*, 4111–4132.
3. Sumida, K.; Stuck, D.; Mino, L.; Chai, J.-D.; Bloch, E.D.; Zavorotynska, O.; Murray, L.J.; Dinca, M.; Chavan, S.; Bordiga, S.; *et al.* Impact of metal and anion substitutions on the hydrogen storage properties of M-BTT metal-organic frameworks. *J. Am. Chem. Soc.* **2013**, *135*, 1083–1091.
4. Dinca, M.; Long, J.R. Hydrogen storage in microporous metal-organic frameworks with exposed metal sites. *Angew. Chem. Int. Ed.* **2008**, *47*, 6766–6779.
5. Rosi, N.L.; Eckert, J.; Eddaoudi, M.; Vodak, D.T.; Kim, J.; O’Keeffe, M.; Yaghi, O.M. Hydrogen storage in microporous metal-organic frameworks. *Science* **2003**, *300*, 1127–1129.
6. Song, Y. New perspectives on potential hydrogen storage materials using high pressure. *Phys. Chem. Chem. Phys.* **2013**, *15*, 14524–14547.
7. Biniwale, R.B.; Rayalu, S.; Devotta, S.; Ichikawa, M. Chemical hydrides: A solution to high capacity hydrogen storage and supply. *Int. J. Hydrogen Energ.* **2008**, *33*, 360–365.
8. Demirci, U.B.; Akdim, O.; Andrieux, J.; Hannauer, J.; Chamoun, R.; Miele, P. Sodium borohydride hydrolysis as hydrogen generator: Issues, state of the art and application upstream from a fuel cell. *Fuel Cells* **2010**, *10*, 335–350.
9. Demirci, U.B.; Miele, P. Sodium borohydride versus ammonia borane, in hydrogen storage and direct fuel cell applications. *Energy Environ. Sci.* **2009**, *2*, 627–637.
10. Lan, R.; Tao, S. Ammonia as a suitable fuel for fuel cells. *Fr. Energy Res.* **2014**, *2*, 35–38.
11. Sanyal, U.; Demirci, U.B.; Jagirdar, B.R.; Miele, P. Hydrolysis of ammonia borane as a hydrogen source: Fundamental issues and potential solutions towards implementation. *Chem. Sus. Chem.* **2011**, *4*, 1731–1739.
12. Jiang, H.-L.; Xu, Q. Catalytic hydrolysis of ammonia borane for chemical hydrogen storage. *Catal. Today* **2011**, *170*, 56–63.
13. Grasemann, M.; Laurenczy, G. Formic acid as a hydrogen source—Recent developments and future trends. *Energy Environ. Sci.* **2012**, *5*, 8171–8181.
14. Klerke, A.; Christensen, C.H.; Norskov, J.K.; Vegge, T. Ammonia for hydrogen storage: Challenges and opportunities. *J. Mater. Chem.* **2008**, *18*, 2304–2310.
15. Cheddie, D. Ammonia as a hydrogen source for fuel cells: A review. In *Hydrogen Energy—Challenges and Perspectives*; INTECH: Rijeka, Croatia, 2012.
16. Holladay, J.D.; Wang, Y. A review of recent advances in numerical simulations of microscale fuel processor for hydrogen production. *J. Power Source* **2015**, *282*, 602–621.
17. Schuth, F.; Palkovits, R.; Schlögl, R.; Su, D.S. Ammonia as a possible element in an energy infrastructure: Catalysts for ammonia decomposition. *Energy Environ. Sci.* **2012**, *5*, 6278–6289.

18. Lan, R.; Irvine, J.T.S.; Tao, S. Ammonia and related chemicals as potential indirect hydrogens storage materials. *Int. J. Hydrogen Energ.* **2012**, *37*, 1482–1494.
19. Rajalakshmi, N.; Jayanth, T.T.; Dhathathreyan, K.S. Effect of carbon dioxide and ammonia on polymer electrolyte membrane fuel cell stack performance. *Fuel Cells* **2004**, *3*, 177–180.
20. Uribe, F.A.; Gottesfeld, S.; Zawodzinski, T.A. Effect of ammonia as potential fuel impurity on proton exchange membrane fuel cell performance. *J. Electrochem. Soc.* **2002**, *149*, 293–296.
21. Yin, S.-F.; Zhang, Q.-H.; Xu, B.-Q.; Zhu, W.-X.; Ng, C.-F.; Au, C.-T. Investigation on the Catalysis of CO_x-free Hydrogen Generation from Ammonia. *J. Catal.* **2004**, *224*, 384–396.
22. Chen, J.; Zhu, Z.H.; Wang, S.; Ma, Q.; Rudolph, V.; Lu, G.Q. Effects of nitrogen doping on the structure of carbon nanotubes (CNTs) and activity of Ru/CNTs in ammonia decomposition. *Chem. Eng. J.* **2010**, *156*, 404–410.
23. Li, L.; Zhu, Z.H.; Yan, Z.F.; Lu, G.Q.; Rintoul, L. Catalytic ammonia decomposition over Ru/carbon catalysts: The importance of the structure of carbon support. *Appl. Catal. A* **2007**, *320*, 166–172.
24. Yin, S.-F.; Xu, B.-Q.; Ng, C.-F.; Au, C.-T. Nano Ru/CNTs: A highly active and stable catalyst for the generation of CO_x-free hydrogen in ammonia decomposition. *Appl. Catal. B* **2004**, *48*, 237–241.
25. Yin, S.-F.; Xu, B.-Q.; Zhou, X.-P.; Au, C.T. A mini-review on ammonia decomposition catalysts for on-site generation of hydrogen for fuel cell applications. *Appl. Catal. A* **2004**, *277*, 1–9.
26. Li, G.; Kanezashi, M.; Lee, H.R.; Maeda, M.; Yoshioka, T.; Tsuru, T. Preparation of a novel bimodal catalytic membrane reactor and its application to ammonia decomposition for CO_x-free hydrogen production. *Int. J. Hydrogen Energ.* **2012**, *37*, 12105–12113.
27. Zheng, W.; Zhang, J.; Xu, H.; Li, W. NH₃ decomposition kinetics on supported Ru clusters: Morphology and particle size effect. *Catal. Lett.* **2007**, *119*, 311–318.
28. Choudhary, T.V.; Sivadinarayana, C.; Goodman, D.W. Catalytic ammonia decomposition: CO_x-free hydrogen production for fuel cell applications. *Catal. Lett.* **2001**, *72*, 197–201.
29. Karim, A.M.; Prasad, V.; Mpourmpakis, G.; Lonergan, W.W.; Frenkel, A.I.; Chen, J.G.; Vlachos, D.G. Correlating particle size and shape of supported Ru/ γ -Al₂O₃ catalysts with NH₃ decomposition activity. *J. Am. Chem. Soc.* **2009**, *131*, 12230–12239.
30. García-García, F.R.; Álvarez-Rodríguez, J.; Rodríguez-Ramos, I.; Guerrero-Ruiz, A. The use of carbon nanotubes with and without nitrogen doping as support for ruthenium catalysts in the ammonia decomposition reaction. *Carbon* **2010**, *48*, 267–276.
31. Armenise, S.; Roldán, L.; Marco, Y.; Monzón, A.; García-Bordejé, E. Elucidation of catalyst support effect for NH₃ decomposition using Ru nanoparticles on nitrogen-functionalized carbon nanofiber monoliths. *J. Phys. Chem. C* **2012**, *116*, 26385–26395.
32. Lee, J.H.; Park, M.J.; Jung, J.; Ryu, J.; Cho, E.; Nam, S.-W.; Kim, J.Y.; Yoon, C.W. Facile synthesis of hollow Fe-N-C hybrid nanostructures for oxygen reduction reactions. *Inorg. Chim. Acta* **2014**, *422*, 3–7.
33. Sun, J.; Zhang, J.; Zhang, M.; Antonietti, M.; Fu, X.; Wang, X. Bioinspired hollow semiconductor nanospheres as photosynthetic nanoparticles. *Nat. Comm.* **2012**, *3*, 1139–1146.
34. Fu, J.; Xu, Q.; Chen, J.; Chen, Z.; Huang, X.; Tang, X. Controlled fabrication of uniform hollow core porous shell carbon spheres by the pyrolysis of core/shell polystyrene/cross-linked polyphosphazene composites. *Chem. Comm.* **2010**, *46*, 6563–6565.

35. Mabudafhasi, M.L.; Bodkin, R.; Nicolaides, C.P.; Liu, X.-Y.; Witcomb, M.J.; Coville, N.J. The ruthenium catalysed synthesis of carbon nanostructures. *Carbon* **2002**, *40*, 2737–2742.
36. Zhang, B.; Qin, X.; Li, G.R.; Gao, X.P. Enhancement of long stability of sulfur cathode by encapsulating sulfur into micropores of carbon spheres. *Energy Environ. Sci.* **2010**, *3*, 1531–1537.
37. Lee, J.H.; Ryu, J.; Kim, J.Y.; Nam, S.-W.; Han, J.H.; Lim, T.-H.; Gautam, S.; Chae, K. H.; Yoon, C.W. Carbon dioxide mediated, reversible chemical hydrogen storage using a Pd nanocatalyst supported on mesoporous graphitic carbon nitride *J. Mater. Chem. A* **2014**, *2*, 9490–9495.
38. Kumar, N.R.S.; Shekar, N.V.C.; Chandra, S.; Basu, J.; Divakar, R.; Sahu, P.C. Synthesis of novel Ru₂C under high pressure-high temperature conditions. *J. Phys. Condens. Matter* **2012**, *24*, 362202–362207.
39. Li, X.; Zhang, J.; Shen, L.; Ma, Y.; Lei, W.; Cui, Q.; Zou, Q. Preparation and characterization of graphitic carbon nitride through pyrolysis of melamine. *Appl. Phys. A* **2009**, *94*, 387–392.
40. Dai, H.; Gao, X.; Liu, E.; Yang, Y.H.; Hou, W.Q.; Kang, L.M.; Fan, J.; Hu, X. Synthesis and characterization of graphitic carbon nitride sub-microspheres using microwave method under mild condition. *J. Diamond Relat. Mater.* **2013**, *38*, 109–117.
41. Li, Y.; Li, T.; Yao, M.; Liu, S. Metal-free nitrogen-doped hollow carbon spheres synthesized by thermal treatment of poly(o-phenylenediamine) for oxygen reduction reaction in direct methanol fuel cell applications. *J. Mater. Chem.* **2012**, *22*, 10911–10917.
42. Jouan, P.-Y.; Peignon, M.-C.; Cardinaud, Ch.; Lempérière, G. Characterisation of TiN coatings and of the TiN/Si interface by X-ray photoelectron spectroscopy and Auger electron spectroscopy. *Appl. Surf. Sci.* **1993**, *68*, 595–603.
43. Campell, D.S.; Leary, H.J.; Slattery, J.S., Jr.; Sargent, R.J. *ESCA Surface Analysis of Plasma Exposed Silicon Nitride and Photoresist Polymer*; IBM General Technology Division: Essex Junction, VT, USA, 1981; pp. 328–329.
44. Bou, M.; Martin, J.M.; Le Mogne, T.; Vovelle, L. Chemistry of the interface between aluminium and polyethyleneterephthalate by XPS. *Appl. Surf. Sci.* **1991**, *47*, 149–161.
45. Sheng, Z.-H.; Shao, L.; Chen, J.-J.; Bao, W.-J.; Wang, F.-B.; Xia, X.-H. Catalyst-free synthesis of nitrogen-doped graphene via thermal annealing graphite oxide with melamine and its excellent electrocatalysis. *ACS Nano* **2011**, *5*, 4350–4358.
46. Byon, H.R.; Suntivich, J.; Shao-Horn, Y. Graphene-based non-noble-metal catalysts for oxygen reduction reaction in acid. *Chem. Mater.* **2011**, *23*, 3421–3428.
47. Carlo, A.D.; Vecchione, L.; Prete, Z.D. Ammonia decomposition over commercial Ru/Al₂O₃ catalyst: An experimental evaluation at different operative pressures and temperatures. *Int. J. Hydrogen. Energ.* **2014**, *39*, 808–814.